Human Identification From Dental X-Ray Images Based on the Shape and Appearance of the Teeth

Omaima Nomir, *Member, IEEE*, and Mohamed Abdel-Mottaleb, *Senior Member, IEEE*

***Abstract*—Dental biometrics deal with human identification from dental characteristics. In this paper, we present a new technique for identifying people based upon shapes and appearances of their teeth from dental X-ray radiographs. The new technique represents each tooth by a feature vector obtained from the forcefield energy function of the grayscale image of the tooth and Fourier descriptors of the contour of the tooth. The feature vector is composed of the distances between a small number of potential energy wells as well as a small number of Fourier descriptors. Given a query image (i.e., postmortem radiograph), each tooth is matched with the archived teeth in the database (antemortem radiographs) that have the same tooth number. Then, voting is used to obtain a list of best matches for the query image based upon the matching results of the individual teeth. Our goal of using appearance and shape-based features together is to overcome the drawback of using only the contour of the tooth, which can be strongly affected by the quality of the images. The experimental results on a database of 162 antemortem images show that our method is effective in identifying individuals based on their dental radiographs.**

***Index Terms*—Antemortem (AM) radiographs, biometrics, dental images, forcefield, forensic odontology, Fourier descriptors, human identification, image segmentation, postmortem (PM) radiographs.**

I. Introduction

FORENSIC radiology is a branch of forensics that deals with identifying people using postmortem radiological images of different parts of the body, including skeleton, skull, and teeth. The branch of forensic radiology that relies on dental radiographs is called forensic odontology [1]. The identification is carried out by comparing postmortem (PM) images with antemortem (AM) records of missing people to find the best match. Dental features are regarded to be the best candidates for postmortem biometric identification. Not only do they represent a unique repository of identifying features, but they are also the most surviving PM part of the victim's body. In other words, the bodies of victims of violent crimes or motor vehicle accidents could be disfigured to such an extent that identification by a family member is neither reliable nor desirable [2]–[6].

Currently, the identification relies on manually comparing extracted features of a PM dental record with the features of AM records archived in a database. Basically, comparative dental identification methods rely on dental restoration and dental work features rather than inherent teeth characteristics (i.e., morphology of the teeth and the roots [7], [8]). Clearly, individuals with numerous and complex dental treatments are often easier to identify than individuals with little or no restorative treatment. Nevertheless, in many cases, these features are not enough to obtian correct identifications [1], [7], [9]. In fact, these features may become unreliable and difficult to use due to advances in dentistry. Consequently, it becomes important to develop automatic dental identification systems using inherent dental features, such as the shapes of the roots and the crowns, and the space between the teeth for substituting the manual methods [10], [11]. Developing automatic dental identification systems caught the attention of a few research groups [12]–[19]. Essentially, an automatic dental biometric system will facilitate for forensic odontologists to search through a large database of AM records and only manually verify the few best matches. To build such a system, there are several challenging issues. These challenges include dealing with poor quality radiographs, which badly affect the segmentation results and, consequently, affect the accuracy of the biometric system. Another challenge is that dental features may change over time, especially if the PM images were captured a long time after the AM images were captured, which leads to difficulty in matching. Small interclass variability for teeth in the same category, for example, two Cuspids from different people, may appear very similar because the X-ray image is a 2-D projection of a 3-D object. Also, another challenge is handling view variance in both AM and PM images.

The contour is one of the important features that can discriminate between teeth. However, due to the poor quality of some images, the resulting contours can have poor quality and this strongly affects the final matching results [18], [20]. In this paper, we present a technique for dental X-ray radiograph matching, which overcomes the drawback of using only the contour of the tooth in matching. It uses features that represent the contour as well as features which describe the appearance of the tooth. The contour is represented using Fourier descriptors, and the appearance is described using a forcefield energy function. Fourier descriptors are calculated for the contour of the tooth; hence, they represent the shape of the contour. On the other hand, the calculation of the forcefield function uses

Manuscript received September 4, 2006. This work was supported in part by the U.S. National Science Foundation under Award EIA-0131079 and in part under Award 2001-RC-CX-K013 from the Office of Justice Programs, National Institute of Justice, U.S. Department of Justice. The associate editor coordinating the review of this manuscript and approving it for publication was Prof. Vijaya Kumar Bhagavatula.

O. Nomir is with the Department of Computer Science, University of Mansoura, El-Mansoura 35516, Egypt.

M. Abdel-Mottaleb is with the Department of Electrical and Computer Engineering, University of Miami, Coral Gables, FL 33146 USA (e-mail: o.nomir@umiami.edu; mottaleb@miami.edu).

Color versions of one or more of the figures in this paper are available online at http://ieeexplore.ieee.org.

Digital Object Identifier 10.1109/TIFS.2007.897245

pixels within the tooth area; hence, it emphasizes the texture. The overall feature vector is the concatenation of the features extracted by the two methods. The extracted features for the AM images are archived in a database. During searching, matching scores are generated based on the distance between the features extracted from the AM and PM teeth. The result of this search is a set of AM candidates that best match the PM query image. We present results that demonstrate the performance of the introduced matching technique. It shows that the technique outperforms the techniques that only use the contour information.

Dental X-ray images are classified according to the view from which they are captured and according to their coverage. The most commonly used images are panoramic, periapical, and bite-wing images [17]. The bite-wing images hold more information about the curvature and the roots, and these images are the most common views made by dentists; therefore, we used them in our system.

The rest of this paper is organized as follows: Section II gives a brief description of the segmentation method. In Section III, we present our new algorithm for matching and retrieval. In Section IV, we study the computational complexity for each step of the proposed matching algorithm. Section V presents the experimental results of the matching technique. Conclusions and future work are discussed in Section VI.

II. Radiograph Segmentation

The goal of radiograph segmentation is to localize the region of each tooth in an X-ray image. Dental radiographs may suffer from poor quality, low contrast, and uneven exposure that complicate the task of segmentation. Dental x-ray images have three different regions: soft tissue regions and background with the lowest intensity values, bone regions with average intensity values, and teeth regions with the highest intensity values. In some cases, the intensity of the bone areas is close to the intensity of the teeth, which makes it difficult to use a single threshold for segmenting the entire image.

We used our segmentation technique introduced in [18]. Fig. 1 shows results on a few bitewing images. The method starts by applying iterative thresholding followed by adaptive thresholding to segment the teeth from both the background and the bone areas. The iterative thresholding starts with an initial threshold estimated from an area around the edges, where the pixels around these areas have high contrast. To obtain a new threshold, the original image is segmented using the initial threshold to separate the image into teeth areas and background areas, and obtain the mean gray values for the two areas. The new threshold is the average of the two mean gray values, and this procedure is repeated until there is no change in the threshold value. The result from the iterative thresholding is a binary image, where detected teeth areas have value one and background areas have value zero. The result of iterative thresholding always includes parts of the bones in the detected teeth areas. To enhance the segmentation results, we follow by applying the adaptive thresholding to the result of masking the original image with the binary image. The adaptive thresholding thresholds a pixel by comparing its value with the average gray value of the nonzero pixels inside a window centered at the given pixel. The final result is also a binary image and the segmentation result is always better than the result obtained by only using the iterative thresholding. After adaptive thresholding, the horizontal integral projection followed by vertical integral projection are applied to separate each individual tooth. The horizontal integral projection separates the upper jaw from the lower jaw, while the vertical integral projection separates each individual tooth in each jaw. To extract the contour points, a connected component analysis using 8-connectivity [21] is applied to obtain the contour pixels of each segmented tooth. For all of the teeth in the database as well as for the PM query teeth, each tooth contour is represented by an equal number of points by applying an equal points sampling technique on the extracted tooth contour pixels.

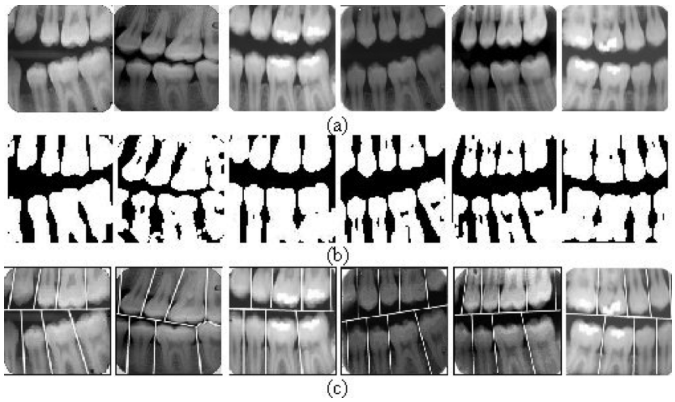

Fig. 1. Teeth segmentation and separation results. (a) The original images. (b) The images after applying adaptive thresholding. (c) The detected separating lines overlaid over the original image.

III. Dental X-Ray Radiograph Matching

Our matching algorithm represents each tooth by a set of features based upon the forcefield energy function and Fourier descriptors. The grayscale image of the tooth is linearly transformed into a forcefield by pretending that each pixel in the image of the tooth exerts an isotropic force on all of the other pixels. There is a potential energy surface associated with this forcefield. The directional property of the forcefield is exploited to automatically locate a small number of potential energy wells that are used to describe each individual tooth. On the other hand, each tooth's contour is represented by the first few Fourier descriptors. Each individual tooth is represented by a feature vector consisting of the normalized distances among the calculated wells concatenated with the Fourier descriptors of the contour of the tooth. Matching scores are generated based on the distance between the AM and the PM feature vectors. The details of the feature extraction step are presented in Section III-A, and the details of the matching step are presented in Section III-B. To increase the accuracy of our matching results and reduce the search space, we consider for matching only corresponding teeth (i.e., teeth that have the same number). For all images in the database, the segmented teeth are automatically classified and numbered according to the universal teeth numbering system using our algorithm described in [19]. This eliminates the possibility of matching teeth that have different numbers.

A. Feature Extraction

This section presents the details for extracting the teeth features. Section III-AI details the analysis and feature extraction using forcefield transformation and Section III-A2 details the feature extraction using Fourier descriptors.

1) Analysis Using Forcefield Transformation: A set of features is extracted to represent each individual tooth. First, the tooth subimage is preprocessed by applying an energy transformation method called forcefield transformation. This transformation was used in [22] for ear recognition—it smoothes the original grayscale image while preserving the important features. In this approach, the 2-D intensity image $f(x,y)$ is treated as a surface. The surface is defined as $w = f(x,y)$, where w is the image intensity at pixel (x,y). Under this representation, the most distinctive features are surface feature points. The algorithm starts by converting a tooth image into a forcefield by pretending that each pixel exerts an isotropic force on all other pixels. Following the gradient direction of the potential energy (5), associated with that forcefield, forms energy lines along the way. Eventually, these energy lines become trapped in a small number of energy wells. These wells are the peaks of the scaler potential energy surface and they are used to describe the appearance of each individual tooth. Assume that each tooth image has N pixels. A pixel i at position r_i with intensity $p(r_i)$ is considered to exert a spherically symmetrical forcefield on surrounding pixels, where the force affecting a pixel j of unit intensity at location r_j is defined as follows:

$$F_i(r_j) = p(r_j) \cdot d_{ji} \tag{1}$$

$$d_{ji} = \frac{(r_i - r_j)}{|r_i - r_j|^3} = \frac{1}{((x_i - x_j)^2 + (y_i - y_j)^2)} \angle\theta \tag{2}$$

where $r_i = [x_i, y_i]$ and $r_j = [x_j, y_j]$, d_{ji} is represented by an absolute value, and an angle $\angle\theta = \tan^{-1}((y_i - y_j)/(x_i - x_j))$, where the angle gives the direction of the forcefield.

This force is associated with a potential energy field $E_i(r_j)$

$$E_i(r_j) = \frac{p(r_i)}{|r_i - r_j|}. \tag{3}$$

The relation between the forcefield function and the energy function can be defined mathematically as follows:

$$F_i(r_j) = \frac{E_i(r_j)}{|r_i - r_j|} \angle\theta. \tag{4}$$

To calculate the total potential energy at a given pixel j, the sum of the potential energy functions from all the pixels within the tooth is taken into account and is given by

$$E(r_j) = \sum_{i=0, i\neq j}^{N-1} E_i(r_j). \tag{5}$$

Fig. 2(b), and (c) shows the potential energy surface, and the top-down view of the energy surface for the tooth image in Fig. 2(a), respectively.

Feature Extraction From the Transformed Image: The forcefield transformation is used to extract a set of features to represent each individual tooth. The feature vector consists of the normalized distances between each pair of wells. To extract

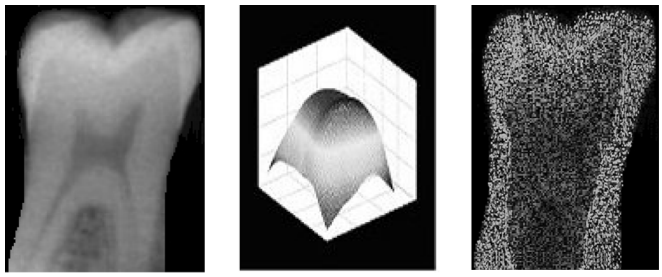

(a) (b) (c)

Fig. 2. Potential energy surface. (a) Tooth image. (b) Potential energy surface. (c) Top-down view of the energy surface for the tooth image in (a).

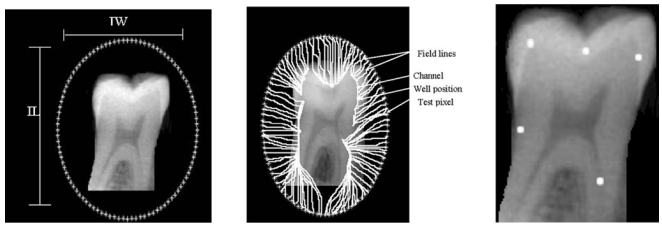

(a) (b) (c)

Fig. 3. Extraction of potential wells. (a) Initialization pixels. (b) Field lines terminating into five wells. (c) Positions of the wells.

the potential wells, an initialization procedure takes place. The initialization procedure starts by arranging a set of 100 pixels [Fig. 3(a)] in an ellipse around each tooth. We chose an ellipse for sampling the initialization pixels because it is the most compact shape that can enclose the tooth and, therefore, the initialization pixels would be at nearly equal distances from the contour of the tooth. The parameters of the ellipse are defined as a function of the length IL and width IW of the tooth image, the major and the minor axes are defined as $(1.2\mathrm{IL})$ and $(1.2\mathrm{IW})$, respectively (i.e., we increase IL and IW by 20% in order to make sure that the tooth image is inside the ellipse). Therefore, the center of the ellipse is at $(1.2\mathrm{IL}/2, 1.2\mathrm{IW}/2)$. We sample the ellipse into N points at equal distances, where each point (x_i, y_i) is defined as follows:

$$x_i = \frac{1.2\mathrm{IL}}{2} + \frac{1.2\mathrm{IL}}{2} \cos\left(\frac{2\pi}{N} i\right), i = 1, \ldots, N \tag{6}$$

$$y_i = \frac{1.2\mathrm{IW}}{2} + \frac{1.2\mathrm{IW}}{2} \sin\left(\frac{2\pi}{N} i\right), i = 1, \ldots, N. \tag{7}$$

After arranging the initialization pixels around each tooth, a procedure is allowed to iteratively follow the gradient of the potential energy, which captures the general flow of the forcefield. By following the field lines [i.e., the paths of the forcefield as in Fig. 3(b)], each field line will continue moving until it reaches a local maximum in the potential energy surface. The field lines flow into a small number of channels. The channel modulates the natural flow of the field lines toward a single well at the center of the field. The flow of the field lines eventually terminates into wells (i.e., the maximum in the potential energy surface), where no force is exerted and no further movement is possible. Fig. 3(c) shows the locations of the wells for the image in Fig. 3(a). Using a set of training data (30 teeth images), we found that initializing the procedure with 100 pixels

TABLE I
RESULTS USING A DIFFERENT NUMBER OF INITIALIZATION PIXELS

# of initialization pixels	Mean(# of wells)	Std(# of wells)
50	5.1	1.398
100	5.966	1.629
150	6.033	1.564
200	6.033	1.564

TABLE II
FIVE NUMBER SUMMARY FOR THE NUMBER OF WELLS

	# of wells
Minimum	3
1st Quartile	4
Median	6
3rd Quartile	7
Maximum	9

is enough for extracting all wells. The result could vary with the number of ellipse points, especially if the number was very small, where some wells would not be detected as no field lines would converge to them. Therefore, the number of initialization pixels should be sufficiently large and evenly distributed to ensure that all wells will be extracted. Table I shows the obtained number of wells, while using a different number of initialization pixels. We can notice that there is a slight difference between the average number of wells when using 100 and 150 initialization pixels. We chose 100 pixels because of the complexity of extracting the wells. We apply this procedure to all images of the AM teeth in the database. Also, the same procedure is applied for the teeth of a given PM image to obtain the corresponding feature vector. Suppose that a tooth has W wells, we define the feature vector as

$$V^t = [d_{1,2}, d_{1,3}, \ldots, d_{W-1,W}], d_{j,k} = \frac{1}{d'}\|w_j - w_k\| \quad (8)$$

where $d_{j,k}$ is the normalized distance between well j, w_j, and well k, w_k; W is the total number of wells; $j = 1, \ldots, W-1$; $k = j+1, \ldots, W$; $j \neq k$, and d' is the mean value of the components of the tooth's feature vector V. d' is used to normalize the distance between each pair of wells (e.g., j and k), to be independent of the scale.

We found from the experimental results, that each tooth has around four to seven wells on average, based on 30 training teeth images. Table II shows the five-number summary for the number of wells ($\mu = 5.966, \sigma = 1.629$).

We store the positions of all the extracted wells for each tooth in our database. During matching, when we match two teeth with a different number of wells, the matching is based on the smallest number of wells as will be explained later in the matching section.

The computational cost for extracting the wells is high since the forcefield calculation uses all pixels within the tooth area. Converting the tooth image into forcefield requires that each pixel exerts an isotropic force on all other pixels, which is time consuming. In order to reduce the computations, we examined the locations of the extracted wells for a set of training teeth images; we found that the wells are usually located in an area around the contour of the tooth. Based on this observation, we only apply the forcefield energy function for a subset of pixels around the tooth's contour. This subset is defined by first defining the center of mass for the tooth. Then, divide the tooth area to the right of the center into two halves, and divide the area to the left of that center into two halves. We choose the two halves (one from the right and one from the left) which are close to the contour. The same procedure is applied to the area above and under the center. The subset to which we apply the forcefield energy function is the union of these selected areas. Fig. 4 shows an example. This tremendously reduces the number of computations compared with the number of computations when we use all of the pixels.

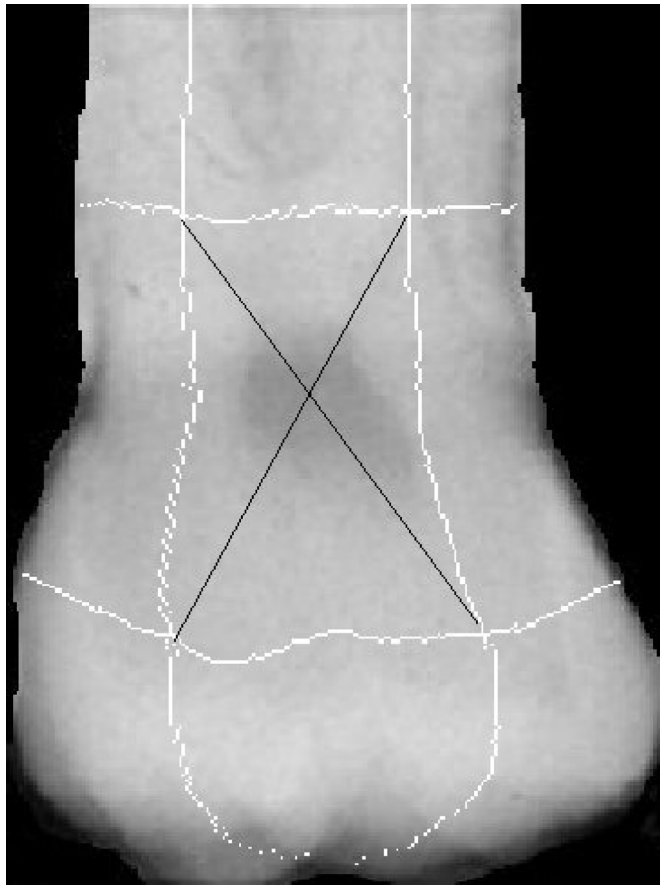

Fig. 4. Force field energy function is applied on a subset of pixels around the tooth's contour (by excluding the area marked with a black X).

2) Feature Extraction Using Fourier Descriptors: Fourier descriptors (FDs) [23]–[25] are powerful for two-dimensional shape description. Considering the 2-D N points of the tooth's contour as a discrete function $u(n) = (x(n), y(n))$ [26], we can define a discrete complex function $f(n)$ to represent the contour of the tooth as

$$f(n) = x(n) + jy(n). \quad (9)$$

By assuming that $f(n)$ is a periodic signal with period N [27], and applying discrete Fourier transformation (DFT) to the complex function, we obtain

$$F(s) = \frac{1}{N}\sum_{i=0}^{N-1} f(i)e^{-2\pi si/N}, s = 0, 1, \ldots, N-1. \quad (10)$$

The coefficients $F(s)$ are called Fourier descriptors. They represent the discrete contour of a shape in the Fourier domain. Since the signal is real, there are only $N/2$ different frequencies in the result of Fourier transformation, and most of the information is in the low-frequency terms. By setting the first Fourier descriptor $F(0)$ to zero, to normalize the location of the centroid of the contour, dividing the remaining coefficients by $F(1)$, and taking only the absolute values of the F's, we can achieve translation invariance, scale invariance, and rotation invariance, respectively [28]–[30]. The feature vector consists of the low-frequency components as follows:

$$V = \left[\frac{|F(2)|}{|F(1)|}, \frac{|F(3)|}{|F(1)|}, \ldots, \frac{|F(21)|}{|F(1)|}\right]. \tag{11}$$

Using a set of training teeth images, we found that the first 20 Fourier descriptors were sufficient to characterize each individual tooth.

B. Teeth Matching

Matching is performed by minimizing the matching distance between the feature vector of the PM tooth and the feature vector of an AM tooth. Suppose we have a query tooth q and a database tooth k and their feature vectors Q and K are defined as

$$Q = [q_i], i = 1, \ldots, \left(\frac{(W-1)W}{2}\right) + 20 \tag{12}$$

$$K = [k_j], j = 1, \ldots, \left(\frac{(W-1)W}{2}\right) + 20 \tag{13}$$

where q_i is the ith feature in the Q vector, k_j is the jth feature in the K vector, W is the number of wells, and $(W-1)W/2$ is the number of features which represent the distances between the wells positions, and the remaining 20 features are the Fourier descriptors.

During matching, the image of a PM tooth is first aligned with that of a corresponding AM tooth [31], [15] (they should also have the same universal tooth number). The alignment step assumes that the image of the PM tooth is transformed with respect to the image of the AM tooth by an affine transformation as follows:

$$T(P) = A \cdot P + \tau \tag{14}$$

where $P = (x, y)^T$ represents a point in the query contour, $T(P)$ is the result of applying the affine transformation on P. A is a transformation matrix that includes both rotation and scaling, and τ is a translation vector as follows:

$$A = \begin{bmatrix} \cos\theta & \sin\theta \\ -\sin\theta & \cos\theta \end{bmatrix} \cdot \begin{bmatrix} S_x & 0 \\ 0 & S_y \end{bmatrix} \tag{15}$$

$$\tau = \begin{bmatrix} \tau_x \\ \tau_y \end{bmatrix} \tag{16}$$

where θ is the rotation angle, S_x and S_y are vertical and horizontal scale factors, and τ_x and τ_y are vertical and horizontal translations. The five parameters, (i.e., θ, S_x, S_y, τ_x, and τ_y) are optimized to obtain the minimum matching distance between the transformed contour of the query tooth and the contour of the AM database tooth. The transformation T is applied to the PM wells positions so that the wells of the PM and AM teeth are also aligned. A sequential quadratic programming optimization method is used to optimize the five parameters [32], [15]. The five parameters are initialized as follows:

$$\theta_0 = \theta_k - \theta_q, S_{x_0} = \frac{W_k}{W_q}, S_{y_0} = \frac{L_k}{L_q},$$
$$\tau_{x_0} = \tau_{k_x} - \tau_{q_x}, \tau_{y_0} = \tau_{k_y} - \tau_{q_y} \tag{17}$$

where θ_k, W_k, and L_k, (τ_{k_x}, and τ_{k_y}) are the orientation of the major axis, the width, the length, and the coordinates of the center for the AM database tooth. Similarly, θ_q, W_q, L_q, (τ_{q_x}, and τ_{q_y}) are the orientation of the major axis, the width, the length, and the coordinates of the center for the PM tooth. The ranges of these five parameters are functions of the initial values, as follows:

$\theta\varepsilon[-2\theta_0, 2\theta_0]$, $S_x\varepsilon[1/S_{x_0}, 2S_{x_0}]$, $S_y\varepsilon[1/S_{y_0}, 2S_{y_0}]$, $\tau_x\varepsilon[-2\tau_{x_0}, 2\tau_{x_0}]$, $\tau_y\varepsilon[-2\tau_{y_0}, 2\tau_{y_0}]$.

The number of extracted wells in both the query and the database teeth may be different. If the number of wells in the query and the database teeth are W_i and W_j, respectively, we only need to compare the corresponding W wells, where

$$W = \min(W_i, W_j). \tag{18}$$

In order to select the W wells, we apply partial directed Hausdorff distance [33] to find the corresponding W wells. The partial directed Hausdorff distance finds the W best matching wells between the PM and the AM teeth. Before applying Hausdorff distance, the PM and AM teeth are aligned, and the positions of the PM wells are transformed using the transformation T. After finding the corresponding wells, the feature vector for each PM tooth is constructed by calculating the distances between the wells for that tooth. These feature vectors are concatenated with the feature vectors obtained by Fourier descriptors, as in (12). The best matches are obtained by finding the AM teeth with the closest feature vectors to the PM query's feature vector.

We applied two matching distance measures to obtain the best matched AM tooth from the database for a given PM query tooth. One method is the $L2$ distance measure (i.e., Euclidean distance, and the second method is the $L1$ distance measure). A comparison between the two methods is given in the experimental section (Section V). The distance between the PM and the AM feature vectors using the Euclidean distance as a function of the transformation T (i.e., rotation, scale and translation), is

$$DE_{T(q),k} = \sqrt{\sum_{i=1}^{((W-1)W/2)+20} (q_i' - k_i)^2} \tag{19}$$

where $T(q)$ is the transformed query tooth, and q_i' is the ith feature of the query tooth after applying the transformation T. The best matching AM tooth, with distance E, will correspond to the minimum $DE_{T(q),k}$

$$E = \text{argmin}_k DE_{T(q),k}. \tag{20}$$

The distance between the PM and AM feature vectors using the $L1$ distance as a function of the transformation T, is

$$DB_{T(q),k} = \sum_{i=1}^{((W-1)W/2)+20} \| (q'_i - k_i) \| . \quad (21)$$

The best matching AM tooth, with distance B, will correspond to the minimum $DB_{T(q),k}$

$$B = \arg\min_k D_{T(q),k}. \quad (22)$$

For both matching methods, in order to obtain the best matching image, majority voting is used so that the best matching AM image is the image with the maximum number of teeth ranked first. For a given PM image, we order the matched AM images according to the maximum number of teeth that rank first, then the maximum number of teeth that rank second and so on. The best AM match is the first image in the list. If there is a tie, the one that has the minimum average matching distance for all of the teeth is chosen. We chose the majority voting method over the total distance method to compare PM and AM images, because in some cases, there is a large distance between one or two corresponding PM and AM teeth for the same person which increases the total matching distance. One reason is the bad quality of some images. Accordingly, this results in incorrectly extracted wells, and/or incorrectly extracted contours for some teeth, hence, a large total distance and a mismatched subject. Using the majority voting overcomes this problem, because it is based on the ranking rather than the distance. When the PM and AM images have good quality, we found that the two methods produce similar results.

IV. Computational Complexity

In this section, we study the space and the time complexity of the introduced technique. For the space complexity, the memory space required for calculating the matching scores between a PM tooth and the AM teeth is equal to the sum of the memory required for N pixels that represent the number of pixels in a tooth image, the memory required for the energy function, the memory required for the feature vectors, and the memory required for M contour points for the AM and PM teeth. In addition, we need to add the memory required for calculating the matching scores. If the size of integer representation is 2 B and the size of float representation is 4 B, then the space complexity S, in bytes, is equal to

$$S = 2(2N + 4N + 4W_1 + 4M) + 4Z \quad (23)$$

where W_1 is the total number of features, which is represented as a constant (small number) and Z is the number of AM teeth. $4Z$ is the number of bytes needed to store the matching scores. The expression for S (i.e., the space complexity for matching a PM query tooth, is equivalent to $O(N)$).

For the time complexity, we calculate the time required for archiving the AM teeth as well as the time required for calculating the matching scores between a PM tooth and the AM teeth. Assume that Z represents the number of AM teeth, M represents the number of contour points, and N represents the number of pixels in a tooth. The time complexity for the archiving step is equal to the time required to extract the wells' positions plus the time required to extract the Fourier descriptors for each AM tooth in the database, which is $O(ZN^2)$ plus $O(ZM \log M)$. Accordingly, the time complexity for the archiving step is $O(ZN^2)$.

For the retrieval step, the time required for calculating the matching scores between a PM tooth and the AM teeth is equal to the sum of the time required to extract the PM wells positions, the time required to extract the Fourier descriptors for the PM tooth, the time required for aligning the PM tooth contour, and each of the AM teeth's contours in the database (that have the same universal tooth number), and the time required for calculating the matching scores, which is equal to

$$C = W(N^2 + M \log M + Z(M^2 + W_1)) \quad (24)$$

where W is constant, and W_1 is the total number of features, which is represented as a constant (small number). The expression for C (i.e., the time complexity for matching a PM query tooth using tooth shape and appearance), is equivalent to $O(N^2)$.

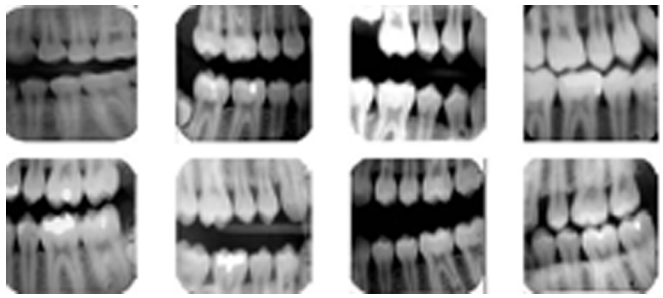

Fig. 5. Sample of the images used in dental image classification.

V. Experiments

In this section, we present the experimental results of our matching algorithm. We used a database from the FBI's Criminal Justice Information Service (CJIS) division, which includes dental radiographs of AM and PM records. Fig. 5 shows a few of the images that we used in the experiments.

The matching method was evaluated using 50 PM query images. The AM database contains 162 AM images. The forcefield energy and the Fourier descriptors of the individual AM teeth were calculated and the feature vectors were extracted and archived in the database. During matching, each segmented tooth in the PM query image is classified and numbered, and its feature vector is calculated and the matching distance is calculated between the PM tooth feature vector and the feature vector of each AM tooth, that has the same number. The best matched (i.e., rank one) AM tooth is the tooth with minimum matching distance. Then, majority voting is used to determine the list of best matching AM images for the query PM image. The voting ranks the AM images according to the ranks of the individual teeth.

Using our database of 162 AM images, the computational time to search for the best matched AM teeth for a given PM

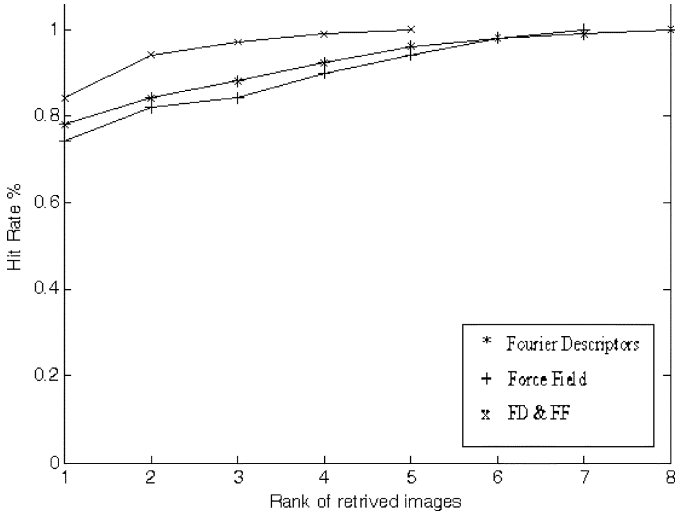

Fig. 6. Matching performance curves.

TABLE III
EXPERIMENTAL RESULTS FOR THE THREE CASES

Method	The number of retrieved images							
	Rank1	Rank2	Rank3	Rank4	Rank5	Rank6	Rank7	Rank8
FF	37	4	1	3		4	1	
FD	39	3	2	2	1	2		1
FF & FD	43	4	2		1			

query tooth in the AM database is 0.56 s, the computational time is based on using the Matlab platform running under a Pentium 4/3.0-GHz processor. Accordingly, the overall computational time to find the list of best matched AM images is the computational time to search for the best-matched AM teeth for a given PM query tooth times the number of teeth in the PM radiograph.

Section V-A presents the results using the Euclidean distance for matching, and Section V-B presents the results using the absolute distance for matching.

A. Matching Using the Euclidean Distance

Using the Euclidean distance, the correct matches were always retrieved for the 50 PM query images, 43 were ranked first, four were ranked second, two were ranked third, and one was ranked fifth. We applied the same matching technique to our testing set, but using only the features obtained from the force-field. The correct matches were also retrieved for the 50 PM query images, 37 were ranked first, four were ranked second, one was ranked third, three were ranked fourth, four were ranked sixth, and one was ranked seventh. We also applied the same matching technique to our test set, but using only the Fourier descriptors as features. The correct matches were also retrieved for the 50 PM query images, 39 were ranked first, three were ranked second, two were ranked third, two were ranked fourth, one was ranked fifth, two were ranked sixth, and one was ranked eighth. We notice that using the two sets of features results in better performance. The matching performance curves for the three cases are shown in Fig. 6. Table III shows the summary of the results.

Fig. 7 shows the retrieval results for one of the query PM images. The left column shows the well positions superimposed on each PM query tooth. The second column shows the corresponding AM teeth for the same subject with the well positions marked. The third and fourth columns show the AM teeth that best match the query teeth along with the complete AM image if the correct AM tooth was not ranked first. The matching distance D is listed under each retrieved tooth. The PM image in Fig. 7 contains seven teeth, where five out of the seven teeth were correctly matched to an AM image of the same person while the correct matches for the two mismatched teeth were ranked second. Majority voting was then used to find the best-matching AM image. In this example, since five out of seven teeth were ranked first and retrieved from the same person, it is considered to be the best match.

We studied the cases that were mismatched; in some cases, the teeth contours, obtained after the segmentation step, were not accurate because of the poor quality of the images. In other cases, the teeth at the image corners have poor quality and are partially visible in the image. Another reason that can affect the results is that the PM images might be captured a long time after the AM images were captured. In this case, the shape of the teeth can change because of artificial prosthesis, teeth growth, or teeth extraction. Table IV summarizes the numbers and the reasons for the mismatched images.

Fig. 8 shows an example of one mismatched result. The correct match for the same person is ranked third. The PM image in Fig. 8(a) contains five teeth., Fig. 8(b) shows that one out of the five teeth was correctly matched to an AM image of the same person (row 1). Also, it shows that four out of the five teeth were matched to the wrong person (rows 2, 3, 4, and 5). Two of these teeth were matched to two teeth in the rank one image (rows 2 and 3). A tie occurred between the three AM images in rows 1, 4, and 5 for the second place. Therefore, we calculated the average matching distance for the three AM images. The AM image that has the minimum average matching distance for all of the matched teeth (i.e., the image in row 4) was chosen. The correct match in this case was ranked third.

Using the same test set, we applied the matching technique based on signature vectors introduced in [18]. This technique relies on selecting a set of salient points on the contour of the tooth and then generates a signature vector for each salient point. The signature vectors capture the curvature information for each salient point. Each element in the vector is the distance between the salient point and a point on the contour. During searching, matching scores are generated based on the distance between the signature vectors of AM and PM teeth. For the 50 PM query images, the correct matches were always retrieved, 40 were ranked first, three were ranked second, two were ranked third, four were ranked fifth, and one was ranked seventh.

Also using the same test set, we applied the matching technique introduced in [20], which matches teeth contours using the hierarchical Chamfer distance. By using the hierarchical representation, the search space is reduced significantly and, consequently, the retrieval time. For the 50 PM query images, the correct matches were always retrieved, 42 were ranked first, three were ranked second, two were ranked fourth, and three were ranked fifth. The matching performance curves for the three techniques are shown in Fig. 9. Also, Table V shows the summary of the results.

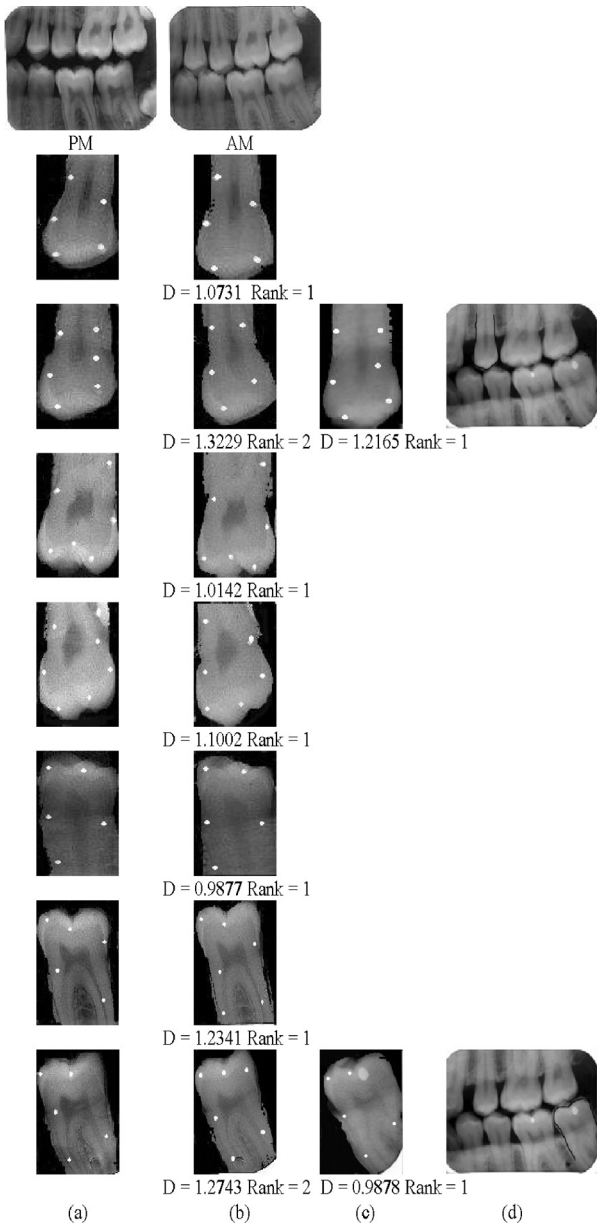

Fig. 7. Retrieval results. (a) A query PM image and the wells positions in each PM tooth. (b) The corresponding AM image for the same person and the wells positions in each matching tooth and its rank. (c) The first-ranked AM tooth if the correct AM tooth was not ranked first. (d) The complete AM image with the tooth in (c) marked with black, if the correct AM tooth was not ranked first.

TABLE IV
NUMBER AND THE REASONS FOR MISMATCHED IMAGES

Reason	# of images
Poor quality of the image	3
PM image captured long time after the corresponding AM image	2
Image corners have poor quality and are partially visible	2

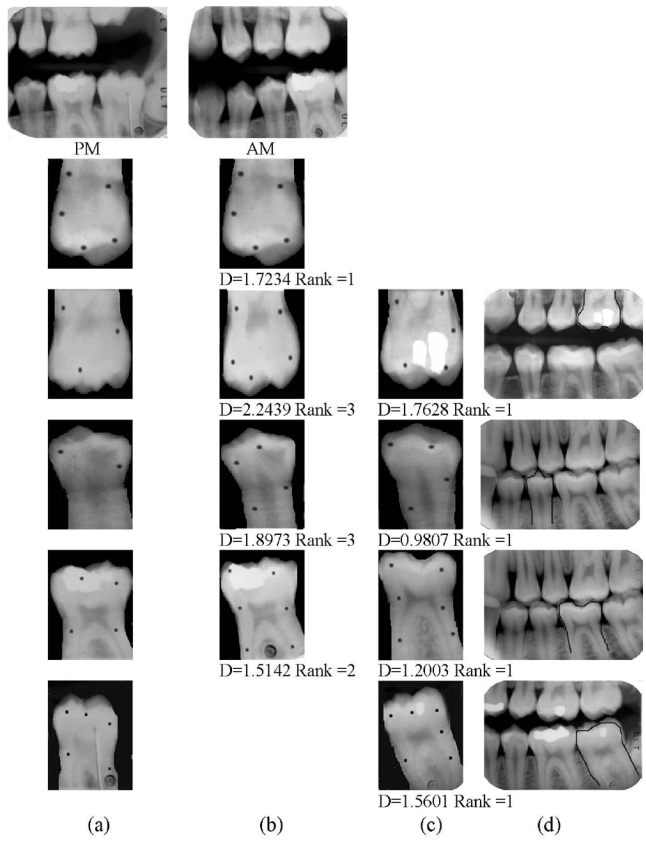

Fig. 8. Retrieval results for a misclassified subject. (a) A query PM image and the wells positions in each PM tooth. (b) The corresponding AM image for the same person and the wells positions in each matching tooth and its rank. (c) The first ranked AM tooth if the correct AM tooth was not ranked first. (d) The complete AM image with the tooth in (c) marked with black if the correct AM tooth was not ranked first.

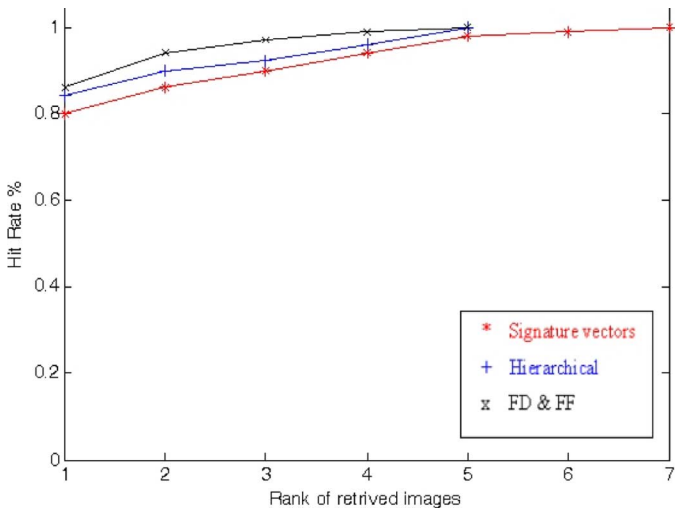

Fig. 9. Performance curves for the three matching methods.

B. Matching Using the Absolute Distance

In this section, we present our results for matching using the absolute distance. For the 50 PM query images, the correct matches were always retrieved for the 50 PM query images, 43 were ranked first, four were ranked second, two were ranked third, and one was ranked fourth. We can notice that there is a slight improvement when we use the absolute distance for matching. Fig. 10 shows the matching performance curves when using the Euclidean and the absolute distances for matching.

To compare the performance between the three matching techniques, we use the ML–One–Err and the ML–coverage

TABLE V
SUMMARY OF THE RESULTS FOR THE THREE MATCHING METHODS

Method	The number of retrieved images						
	Rank 1	Rank 2	Rank 3	Rank 4	Rank 5	Rank 6	Rank 7
Signature vectors	40	3	2		4		1
Hierarchical	42	3		2	3		
FF & FD	43	4	2		1		

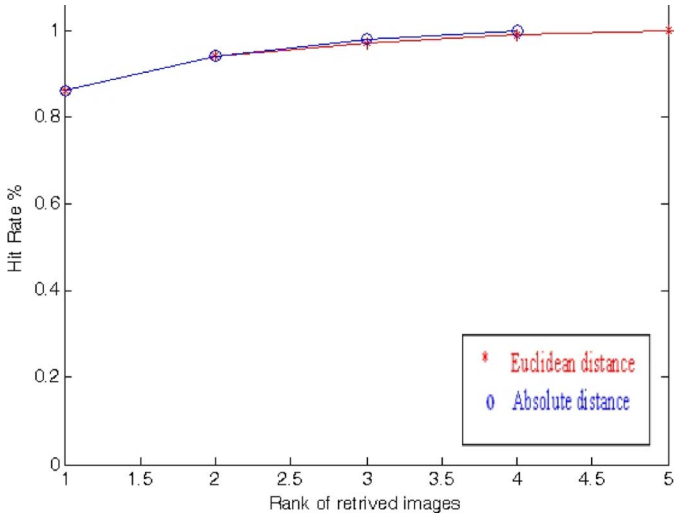

Fig. 10. Matching performance curves when using the Euclidean and the absolute distances for matching.

measures, which are commonly used in multilabel environments [34], [35] to compare between the performance of more than one classifier. These two measures are defined as follows:

$$\mathrm{ML-One-Err} = \frac{\bigcup\{x \varepsilon X : r_x \neq 1\}}{|X|} \tag{25}$$

where x is a query image, X is the set of all query images, r_x is the rank of image x, $\bigcup$ is the number of images with $r_x \neq 1$, and $|X|$ is the total number of query images

$$\mathrm{ML-Coverage} = \frac{\sum_{x \varepsilon X} (r_x - 1)}{|X|} \tag{26}$$

where x is a query image, X is the set of all query images, r_x is the rank of image x, and $|X|$ is the total number of query images. Small values of these measures indicate better performance. The range for the ML–One–Err is from zero to one, while for the ML–Coverage measure, it is zero for perfect performance and increases with lower performance.

Table VI shows the results when using the Euclidean and absolute distances for matching. We can notice that Hierarchical matching outperforms the matching using signature vectors. Matching using forcefield and Fourier descriptors outperforms the matching using signature vectors and the hierarchical matching.

VI. CONCLUSION

In this paper, we introduced an algorithm for matching dental X-ray images. We used bitewing X-ray images, because they are the most common views made by dentists. The algorithm extracts a small set of features, for each tooth, that represents the appearance of the tooth as well as the shape of the contour of the tooth. This overcomes the drawback of representing the tooth by only the contour information, which can be affected by the poor quality of some of the images. Given a PM query image, matching scores are calculated based on the distance between the feature vectors extracted from the PM tooth and each AM tooth (that have the same tooth number). Then, voting is used to obtain a ranked list of best matches for the query PM image based on the matching results of the individual teeth. We have shown experimental results for the matching technique on images of different qualities. We have also shown that the new technique outperforms our previous techniques that only use the contours of the teeth for matching.

In our future work, we will extend our system to handle panoramic and periapical radiographs, and develop algorithms for fast retrieval.

TABLE VI
PERFORMANCE EVALUATION FOR THE THREE METHODS

Method	The used matching distance			
	Euclidean		Absolute	
	ML-One-Err	ML-Coverage	ML-One-Err	ML-Coverage
Signature vectors	0.20	0.58	0.20	0.58
Hierarchical	0.16	0.42	0.14	0.38
FF & FD	0.14	0.24	0.14	0.22

REFERENCES

[1] "American society of forensic odontology," *Forensic Odontology News*, vol. 16, no. 2, 1997.
[2] F. S. Malkowski, "Forensic dentistry, A study of personal identification," *Dental Study*, vol. 51, pp. 42–44, 1972.
[3] V. W. Weedn, "Postmortem identifications of remains," *Clin. Lab. Med.*, vol. 18, pp. 115–137, 1998.
[4] R. B. Dorion, "Disasters big and small," *J. Can. Dental Assoc.*, vol. 56, pp. 593–598, 1990.
[5] L. Hong, A. K. Jain, and S. Pankanti, "Biometric identification," *Commun. ACM*, vol. 43, no. 2, 2000.
[6] S. Pankanti, R. Bolle, and A. K. Jain, "Biometric: The future of identification," *IEEE Comput.*, vol. 33, no. 2, pp. 46–49, Feb. 2000.
[7] "Computer assisted postmortem identification via dental and other characteristics," in *USAIDR*. Washington, D.C.: United States Army Inst. Dental Res. Walter Reed Army Medical Center, 1990, vol. 5.
[8] B. G. Brogdon, *Forensic Radiology*. Boca Raton, FL: CRC, 1998.
[9] D. J. McGivney *et al.*, WinID2 Software [Online]. Available: www.winid.com.
[10] P. Stimson and C. Mertz, *Forensic Dentistry*. Boca Raton, FL: CRC, 1997.
[11] Gustafson and Ghosta, *Forensic Odontology*. New York: American Elsevier, 1996.
[12] A. K. Jain and H. Chen, "Dental biometrics: Alignment and matching of dental radiographs," *IEEE Trans. Pattren Anal. Mach. Intell.*, vol. 27, no. 8, pp. 1319–1326, Aug. 2005.
[13] A. K. Jain and H. Chen, "Matching of dental x-ray images for human identification," *Pattern Recognit.*, pp. 1519–1532, Jul. 2004.
[14] M. Abdel-Mottaleb, O. Nomir, D. E. Nassar, G. Fahmy, and H. H. Ammar, "Challenges of developing an automated dental identification system," presented at the IEEE Midwest Symp. Circuits Syst., 2003.
[15] A. K. Jain, H. Chen, and S. Minut, "Dental biometrics: Human identification using dental radiographs," in *AVBPA*, Guildford, U.K., 2003, pp. 429–437.
[16] G. Fahmy, D. Nassar, E. Haj-Said, H. Chen, O. Nomir, J. D. Zhou, R. Howell, H. H. Ammar, M. Abdel-Mottaleb, and A. K. Jain, "Towards an automated dental identification system (adis)," in *Proc. ICBA*, 2004, pp. 789–796.
[17] J. D. Zhou and M. Abdel-Mottaleb, "A content-based system for human identification based on bitewing dental x-ray images," *Pattern Recognit.*, vol. 38, pp. 2132–2142, Nov. 2005.
[18] O. Nomir and M. Abdel-Mottaleb, "A system for human identification from x-ray dental radiographs," *Pattern Recognit.*, vol. 38, pp. 1295–1305, Aug. 2005.

[19] M. Mahoor and M. Abdel-Mottaleb, "Classification and numbering of teeth in bitewing dental images," *Pattern Recognit.*, vol. 38, pp. 577–586, Apr. 2005.
[20] O. Nomir and M. Abdel-Mottaleb, "Hierarchical dental x-ray radiographs matching," in *Proc. ICIP*, Oct. 2006, pp. 2677–2680.
[21] R. Gonzalez and R. Wood, *Digital Image Process.* Reading, MA: Addison-Wesley, 1993.
[22] D. Hurley, M. Nixon, and J. Carter, "A new force field transform for ear and face recognition," in *Proc. ICIP*, 2000, pp. 25–28.
[23] R. L. Cosgriff, "Identification of Shape," Tech. Rep., Ohio State Univ., Columbus, OH, 1990.
[24] D. Hurley, M. Nixon, and J. Carter, "An experimental comparison of autoregressive and Fourier-based descriptors in 2d shape classification," *IEEE Trans. Pattern Anal. Mach. Intell.*, vol. 17, no. 2, pp. 201–207, Feb. 1995.
[25] R. O. Duda and P. E. Hart, *Pattern Classification and Scene Analysis*. New York: Wiley, 2000.
[26] K. Arbter, W. E. Snyder, H. Burhardt, and G. Hirzinge, "Content-based image retrieval using Fourier descriptors on a logo database," *Pattern Recognit.*, vol. 3, pp. 521–524, Aug. 2002.
[27] K. Arbter, W. E. Snyder, H. Burhardt, and G. Hirzinge, "Application of affine-invariant Fourier descriptors to recognition of 3d objects," *IEEE Trans. Pattern Anal. Mach. Intell.*, vol. 12, no. 12, pp. 640–647, Dec. 1990.
[28] L. F. Costa and R. M. Cesar, *Shape Analysis and Classification: Theory and Practice*. Boca Raton, FL: CRC, 2000.
[29] R. Chellappa and R. Bagdazian, "Fourier coding of image boundaries," *IEEE Trans. Pattern Anal. Mach. Intell.*, vol. PAMI-6, no. 1, pp. 102–105, Jan. 1984.
[30] D. Zhang and G. Lu, "A comparative study on shape retrieval using Fourier descriptors with different shape signatures," in *Proc. Conf. Intelligent Multimedia and Distance Education*, 2001, pp. 1–9.
[31] T. Cootes and C. Taylor, "Statistical Models of Appearance for Computer Vision," Tech. Rep. Imaging Sci. Biomedical Eng., Wolfson Image Analysis Unit, Univ. Manchester, , Manchester, U.K., 2000.
[32] S. P. Han, "A globally convergent method for nonlinear programming," *Optim. Theory Appl.*, vol. 22, no. 3, pp. 297–309, 1977.
[33] D. P. Huttenlocher, G. A. Klanderman, and W. J. Ruchlidge, "Comparing images using the Hausdorff distance," *Pattern Recognit.*, vol. 15, no. 9, pp. 850–862, 1993.
[34] F. J. Provost, "Robust classification for imprecise environments," *Mach. Learning*, vol. 42, no. 3, pp. 203–231, 2001.
[35] R. E. Shapire and Y. Singer, "Boostexter: A boosting-based system for text categorization," *Mach. Learning*, vol. 39, pp. 135–168, 2000.

Omaima Nomir (M'07) received the Ph.D. degree in electrical and computer engineering from University of Miami, Coral Gables, FL, in 2006.

Her research interests include human identification, pattern recognition, medical image processing, and neural networks. She has published ten research papers.

Mohamed Abdel-Mottaleb (SM'03) received the Ph.D. degree in computer science from the University of Maryland, College Park, in 1993.

Currently, he is an Associate Professor in the Department of Electrical Computer Engineering, University of Miami, Cora Gables, FL, where his research focuses on 3-D face recognition, dental biometrics, visual tracking, and human activity recognition. Prior to joining the University of Miami, from 1993 to 2000, he was with Philips Research, Briarcliff Manor, NY, where he was a Principal Member of the Research Staff and a Project Leader, where he led several projects in image processing and content-based multimedia retrieval. He holds 20 U.S. patents and has published many papers in the areas of image processing, computer vision, and content-based retrieval.

Dr. Abdel-Mottaleb is an Associate Editor for *Pattern Recognition* journal.